Journal of Solid State Chemistry 230 (2015) 175–181

Contents lists available at ScienceDirect

Journal of Solid State Chemistry

journal homepage: www.elsevier.com/locate/jssc

Importance of the tuning of band position in optimizing the electronic coupling and photocatalytic activity of nanocomposite

Xiaoyan Jin [a], Eun Kyung Mok [a], Ji-Won Baek [a], Sang-Hyun Park [b], Seong-Ju Hwang [a,*]

[a] Department of Chemistry and Nanoscience, College of Natural Sciences, Ewha Womans University, Seoul 120-750, Republic of Korea
[b] Smithers-Oasis Korea, 196-4 YongJungDoHa-Gil 157, Cheonan, Chungnum-Do, Republic of Korea

ARTICLE INFO

Article history:
Received 2 May 2015
Received in revised form
3 July 2015
Accepted 6 July 2015
Available online 9 July 2015

Keywords:
Nitrogen doping
Electronic coupling
Nanocomposite
Photocatalytic activity
Titanium oxide

ABSTRACT

The electronic coupling and photocatalytic activity of Ag_2CO_3–TiO_2 nanocomposite can be optimized by the fine-tuning of the band position of titanium oxide with nitrogen doping. The increase of the valence band energy of TiO_2 by N-doping leads not only to the enhanced absorption of visible light but also to the promoted hole transfer from Ag_2CO_3 to TiO_2, resulting in the efficient spatial separation of photogenerated electrons and holes. While the undoped Ag_2CO_3–TiO_2 nanocomposite shows an inferior photocatalytic activity to the pure Ag_2CO_3, the photocatalyst performance of N-doped nanocomposite is better than those of Ag_2CO_3 and undoped Ag_2CO_3–TiO_2 nanocomposite. This observation underscores a significant enhancement of the photocatalytic activity of nanocomposite upon N-doping, a result of enhanced electronic coupling between the hybridized species. The present results clearly demonstrate the importance of the fine-tuning of band position in optimizing the photocatalytic activity of hybrid-type photocatalysts.

1. Introduction

Semiconductor-based photocatalysts attract a great deal of research interest as eco-friendly options for producing renewable energy sources and also for purifying environmental pollutions [1–5]. Since most of metal oxide-based semiconductors such as TiO_2 possess large bandgap energy of >3 eV, these materials cannot harvest visible light energy and thus suffer from poor photoefficiency [6,7]. To circumvent the drawback of metal oxide-based photocatalysts, many kinds of strategies are developed such as dye sensitization, chemical substitution, and so on [8–10]. Hybridization between two kinds of semiconductors can provide one of the most effective ways to explore new efficient visible light photocatalysts [10–12]. Since silver oxosalts like Ag_2CO_3 show strong visible light absorption and unusually high photocatalytic activity [13], these materials can be used as partners for coupling with wide bandgap semiconductor to synthesize new type of visible light active photocatalyst. In the resulting nanocomposite, an electronic coupling between the components is of prime importance in optimizing its photocatalytic activity [14], since the efficient electron coupling between these components makes possible the harnessing of visible light energy and the depression of the recombination between excited electrons and holes [14]. It is fairly crucial to match the band positions of hybridized semiconductors for achieving a strong electronic coupling between them. In one instance, the Ag_2CO_3–TiO_2 nanocomposite suffers from the mismatch of the band positions of the component semiconductors, which frustrates an efficient electronic coupling between them. That is, the valence band (VB) of Ag_2CO_3 has a slightly higher position than does that of TiO_2, whereas the conduction band (CB) of Ag_2CO_3 is located in a lower position than that of TiO_2 [15,16]. Hence, the hole in the VB of Ag_2CO_3 cannot be efficiently transferred to that of TiO_2, resulting in a poor electronic coupling between these semiconducting components. To circumvent the mismatch of electronic structures, it must be effective to elevate the VB position of TiO_2 through the partial replacement of oxygen with electropositive nitrogen [17]. The resulting higher VB energy of N-doped TiO_2 is supposed to allow an efficient hole transfer from Ag_2CO_3 to TiO_2, resulting in the spatial separation of photogenerated electrons and holes. However, there is no report about the optimization of the electronic coupling and photocatalytic activity of silver oxosalt–metal oxide nanocomposite through the anion doping.

In this study, the effect of anion doping on the electronic coupling and photocatalytic activity of Ag_2CO_3–TiO_2 nanocomposite (denoted as **ACT**) is investigated. The electronic structure and physicochemical properties of Ag_2CO_3–N-doped TiO_2 nanocomposite (denoted as **ACNT**) are compared with undoped **ACT** homolog. Also, the evolution of photocatalytic activity upon the nitrogen doping is examined by monitoring the decomposition of

* Corresponding author.
E-mail address: hwangsju@ewha.ac.kr (S.-J. Hwang).

http://dx.doi.org/10.1016/j.jssc.2015.07.006
0022-4596/

organic molecules under visible irradiation.

2. Materials and methods

2.1. Materials

The **ACT** nanocomposite was prepared by the hybridization between TiO_2 and Ag_2CO_3, in which the static adsorption effect plays an important role in the combination process of two building blocks; 0.25 g of P25 (Degussa P25) powder was dispersed in 20 mL of distilled water, and then 7.8 mL of 0.1 M $NaHCO_3$ solution was added to P25 suspension under stirring for 10 min. Finally, 15.6 mL of 0.1 M $AgNO_3$ solution was reacted with the suspension of P25 and $NaHCO_3$. The molar ratio of TiO_2:Ag_2CO_3 was fixed as 1:0.25. The obtained precipitate of **ACT** nanocomposite was washed with distilled water and dried. The N-doped homolog of **ACNT** nanocomposite was obtained by the same synthetic process except for the use of N-doped TiO_2 nanoparticles. The pure Ag_2CO_3 was also synthesized by the same synthetic method as that for the **ACT** nanocomposites except for the absence of P25. The nitrogen doping for the precursor P25 TiO_2 was accomplished by the heat-treatment of the as-purchased P25 powder in NH_3 flow at 600 °C for 4 h, as reported previously [18].

2.2. Characterization

The crystal structure of the obtained nanocomposites was probed with powder X-ray diffraction (XRD) analysis (Rigaku D/Max-2000/PC, Ni-filtered Cu Kα radiation, 298 K). The crystal morphology and elemental compositions of the obtained materials were examined with field emission-scanning electron microscopy (FE-SEM) and energy dispersive spectrometry (EDS) – elemental mapping analysis using Jeol JSM-6700F microscope equipped with an energy dispersive X-ray spectrometer. The transmission electron microscopy (TEM) images of the present nanocomposites were collected with a Jeol JEM-2100F microscope at an accelerating voltage of 200 kV. The evolution of the surface area upon nanocomposite formation was studied by measuring N_2 adsorption–desorption isotherms at 77 K with an ASAP 2020 analyzer. The electronic structure of the present materials was investigated by diffuse reflectance UV–vis spectroscopy using a Perkin-Elmer Lambda 35 spectrometer. $BaSO_4$ was utilized as a reference. The internal charge transfer in the present nanocomposites was studied with photoluminescence (PL) spectroscopy using Perkin-Elmer LS55 fluorescence spectrometer. The X-ray photoelectron spectroscopy (XPS) data were collected by XPS machine (Thermo VG, UK, Al K_α), whose energies were referenced to the adventitious C 1s peak at 284.8 eV. The zeta potentials of the photocatalyst suspensions were measured with Malvern Zetasizer Nano ZS (Malvern, UK).

2.3. Photocatalytic activity measurements

The photocatalytic activity of the present materials was tested under visible light irradiation ($\lambda > 420$ nm). Prior to the photocatalyst test, the organic substrate molecule was added to an aqueous photocatalyst suspension in a glass reactor with a quartz window and then equilibrated with stirring for 30 min in the dark condition to minimize the effect of the surface adsorption of substrate molecules. Light from a 450 W arc lamp (Oriel) was passed through water and cutoff filter to eliminate IR and UV radiation, respectively. For the photodegradation tests of organic molecules, 50 μM methylene blue (MB) and 50 μM 4-chlorophenol (4-CP) were used as target materials and 30 mg of the photocatalysts were used for each test. Sample aliquots were drawn by a 1 mL syringe intermittently during the photoreaction and filtered through a 0.45 μm PTFE filter (Whatman) to remove catalyst particles. The concentration of MB was estimated with a UV–vis spectrophotometer (Agilent 8453). The concentration of 4-CP was measured with a reverse-phase high performance liquid chromatograph (HPLC, Agilent 1100 series). The eluent solution was composed of deionized water (60%) and acetonitrile (40%).

3. Result and discussion

3.1. XRD analysis

The powder X-ray diffraction (XRD) patterns of the **ACT** and **ACNT** nanocomposites and the precursors of undoped and N-doped P25 TiO_2, and Ag_2CO_3 are plotted in Fig. 1. The undoped P25 TiO_2 shows the Bragg reflections of anatase and rutile TiO_2 phases, indicating the co-existence of both TiO_2 phases in this material [19]. The N-doping for the P25 TiO_2 precursor does not cause any significant change of the XRD pattern, confirming no marked influence of N-doping on the crystal structure of P25 precursor. The **ACT** nanocomposite displays the XRD peaks of Ag_2CO_3, anatase TiO_2, and rutile TiO_2 phases, clearly demonstrating the composite formation of silver carbonate and titanium oxides. The intensity ratio of anatase TiO_2/rutile TiO_2 Bragg reflections remains the same as the precursor P25, confirming the maintenance of the crystal structure of P25 upon the composite formation with Ag_2CO_3. Nearly identical XRD patterns are observed for both the **ACT** and **ACNT** nanocomposites, underscoring no significant variation of the composite structure upon N-doping. According to the particle size calculation based on the Scherrer equation, the N-doping and the composite formation with Ag_2CO_3 have negligible effects on the particle size of the precursor P25 (20 nm for anatase TiO_2 component, 28 nm for rutile TiO_2 component), showing no change of particle size of TiO_2 phases.

3.2. FE-SEM, HR-TEM, and EDS-mapping analyses

Fig. 2A–E represents the field emission-scanning electron microscopy (FE-SEM) images of the **ACT** and **ACNT** nanocomposites and the precursors of undoped and N-doped P25 TiO_2 and Ag_2CO_3. Both the undoped and N-doped TiO_2 precursors commonly show

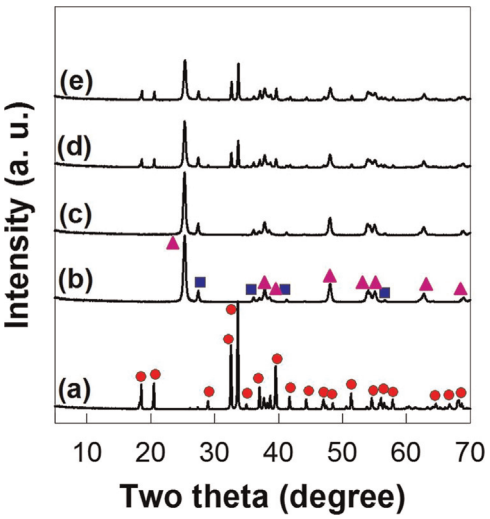

Fig. 1. Powder XRD patterns of (a) Ag_2CO_3, (b) P25 TiO_2, (c) N-doped P25 TiO_2, (d) **ACT** nanocomposite, and (e) **ACNT** nanocomposite. The circles, triangles, and squares denote the Bragg reflections of Ag_2CO_3, anatase TiO_2, and rutile TiO_2 components, respectively.